The 2nd Spitzer Conference: Infrared Diagnostics of Galaxy Evolution
ASP Conference Series, Vol. 381, ©2008
Ranga-Ram Chary, Harry I. Teplitz, Kartik Sheth, eds.

GOODS *Spitzer*/IRAC Observations of High-z Galaxies

Haojing Yan,[1] Mark Dickinson,[2] Mauro Giavalisco,[3] Daniel Stern,[4] Peter R. M. Eisenhardt,[4] Henry C. Ferguson[3] and the GOODS Team

[1] *Spitzer Science Center, California Institute of Technology, MS 220-6, Pasadena, CA 91125*
[2] *National Optical Astronomy Observatory, 950 North Cherry Street, Tucson, AZ 85719*
[3] *Space Telescope Science Institute, Baltimore, MD 21218*
[4] *Jet Propulsion Laboratory, California Institute of Technology, Pasadena, CA 91109*

Abstract. The Great Observatory Origins Deep Survey (GOODS) *Spitzer* Legacy Program has obtained ~ 23.2 hours of IRAC observations in the HDF-N and the CDF-S ($\sim$ 330 arcmin^2 in total), among which a sub-area of $\sim$ 50 arcmin^2 in the HDF-N has been observed to a depth of ~ 72 hours. Utilizing these deep IRAC data, we study the stellar masses and star formation histories of galaxies at $z \approx 6$. While some of the i-band dropouts selected by the GOODS ACS observations are detected by these IRAC observations, some of them are not. We find that the i_{775}-dropouts in the IRAC-detected sample typically have stellar masses of $\sim 10^{10} M_{\odot}$ and ages of a few hundred million years old, consistent with our earlier results based on a smaller sample in the HUDF. On the other hand, the i-dropouts in the IRAC-invisible sample are significantly younger and less massive. Using these results, we derive the lower limit of the global stellar density at $z \approx 6$, and find that at least 0.2–1.1% of the stellar mass in our local universe has been locked in stars by $z \approx 6$.

1. Introduction

The Infrared Array Camera (IRAC; Fazio et al. 2004) of the *Spitzer Space Telescope* (Werner et al. 2004) has opened up a new window for the study of galaxies at very high redshifts. Its impressive sensitivity in the 3.6 and 4.5 μm channels enables the detection of galaxies as distant as $z \approx 6$, and thus, for the first time, offers the unique opportunity of investigating the rest-frame optical properties of galaxies in the early universe. At these wavelengths, the light from a galaxy is less affected by dust extinction and is more sensitive to the longer-lived stars that dominate the stellar mass. For these reasons, IRAC observations can provide a wealth of information about the stellar population of galaxies at very high redshifts, such as their ages and stellar masses. The deep IRAC data obtained by the Great Observatory Origins Deep Survey (GOODS) *Spitzer* Legacy (Dickinson et al., in preparation) are unparalleled for this purpose.

Previously, we used the first-epoch of GOODS IRAC data to study three $z \approx 6$ and eleven $z \approx 5$ galaxies in the HUDF (Yan et al. 2005), and found that some galaxies as massive as $\sim 10^{10} M_{\odot}$ were already in place when the universe was only ~ 1 Gyr old, and that their ages were about a few hundred years (see also Eyles et al. 2005). While the existence of such high-mass galaxies in the early universe seemingly conflicts the hierarchical formation theory, we found

that their number density actually could be explained by at least one set of ΛCDM simulations (e.g., Negamine et al. 2005).

In this study, we extend our previous work to the entire GOODS fields by studying all the i_{775}-band dropouts selected by the GOODS ACS observations. We utilize the full, two-epoch IRAC data that cover the HDF-N and the CDF-S to a depth of ~ 23.2 hours (~ 330 arcmin^2 in total; here after the "super-deep" data) as well as the deeper IRAC data that cover a sub-area of ~ 50 arcmin^2 in the HDF-N a depth of ~ 72 hours (hereafter the "ultra-deep" data). The preliminary results from this study is presented below. Throughout this paper, we adopt the following cosmological parameters (Spergal et al. 2003): $\Omega_M = 0.27$, $\Omega_\Lambda = 0.73$, and $H_0 = 71$ km s^{-1} Mpc^{-1} ($h = 0.71$).

2. GOODS i_{775}-Dropouts and their IRAC Detections

The $z \approx 6$ galaxy candidates used in this paper are the i-dropouts selected from the complete, 5-epoch GOODS ACS observations in both the HDF-N and CDF-S (Giavalisco et al. 2004a). Briefly, the selection criteria are: $S/N \geq 5$ in z_{850}, $(i_{775} - z_{850}) > 1.3$ mag, and $S/N < 2$ in both the V_{606} and B_{435} (see also Giavalisco et al. 2004b; Dickinson et al. 2004). To minimize the contamination caused by Galactic brown dwarfs, we exclude objects with FWHM$< 0.12''$.

The i_{775}-dropouts were cross-matched with the IRAC sources detected in the super-deep data, following the procedures adopted in Yan et al. (2004; 2005). As the FWHM of the point spread function (PSF) in the 3.6μm channel is about $1.8''$, the matching of the high-z galaxy candidates and the IRAC sources was done with a $2''$ search radius. The matched sources were then visually inspected to ensure that the identifications were secure. In order to avoid ambiguity in interpreting the measured fluxes, we excluded any IRAC sources that are blended with foreground objects. A number of i_{775}-dropouts have very bright counterparts in the IRAC images, giving flux density ratios $f_\nu(3.6\mu m)/f_\nu(z_{850}) > 20$. Thus they satisfy the selection criterion of the "IRAC-selected Extremely Red Objects" (IEROs; Yan et al. 2004), which are likely old, passively-evolving galaxies at $z \approx 2.4$. Therefore, these objects are rejected from the sample. The final "IRAC-detected" sample consists of 34 and 19 objects in the CDF-S and the HDF-N, respectively.

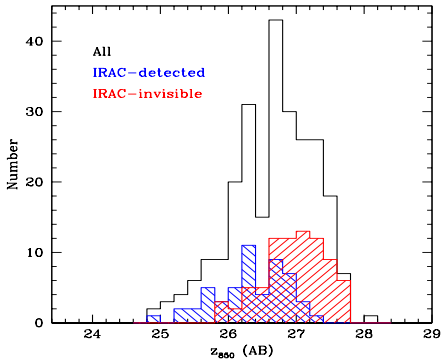

Fig. 1 The distribution of z_{850} magnitudes of the i_{775}-dropouts in the GOODS fields. The black, unfilled histograms are for all objects, while the shaded blue

and red histograms are for the IRAC-detected and IRAC-invisible samples, respectively.

We visually examined the IRAC images at the positions of the i_{775}-dropouts that were not cross-matched in the above procedure and found that 45 objects in the CDF-S and 34 objects in the HDF-N were undetected because of their faintness — quantitatively, they all have $S/N < 3$ in both the 3.6 and 4.5 μm images. We refer to this sample as the "IRAC-invisible" sample.

The objects in the IRAC-detected and IRAC-invisible samples are not distinctly different. Their rest-frame UV luminosities (and hence their ongoing star activities), represented by their z_{850} magnitudes, significantly overlaps (Fig. 1). Their luminosity difference in the IRAC passbands is more a result of the difference in their stellar masses, which is the subject that we will discuss below. The ultra-deep observations detects at least one object in the IRAC-invisible sample (see below), which indicates a smooth transition of the IRAC properties of these objects from one sample to the other.

3. Constraining the Stellar Masses of $z \approx 6$ Galaxies

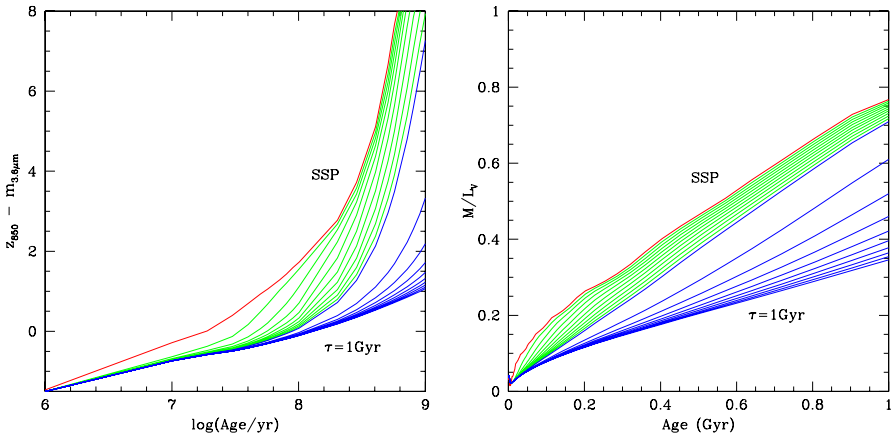

Fig. 2 (left) The evolution of $(z_{850} - m_{3.6\mu m})$ color for the models considered in our study. For a given color, an age can be inferred for a particular model, and thus we can compare our observation to the prediction of this model at the inferred age and obtain a mass estimate. The minimum mass obtained among all the models is $M_{\rm min}$, while the median value is referred to as $M_{\rm rep}$.
Fig. 3 (right) The evolution of M/L of the models. At the maximum age allowed by our adopted cosmology ($\sim$ 1 Gyr), a SSP reaches the largest possible M/L among all the models, and thus gives the highest possible stellar mass for a given luminosity.

We constrain the stellar masses of $z \approx 6$ galaxies in both the IRAC-detected and the IRAC-invisible samples by comparing our observations to the stellar population synthesis models of Bruzual & Charlot (2003; hereafter BC03). Following Yan et al. (2005), we explore the models of these star formation histories (SFHs): instantaneous bursts (or Simple Stellar Populations, SSPs), and continuous bursts with exponentially declining star formation rate (SFR) in the form

of $SFR \propto \tau^{-1}\ exp(t/\tau)$, where the time-scale τ ranges from $\tau = 10$ Myr to 1 Gyr. The step size in τ is 10 Myr for $\tau = 10$ Myr to 0.1 Gyr, and is 0.1 Gyr for $\tau = 0.1$ to 1 Gyr. For each of these SFHs, we generate models with ages ranging from 1 Myr to 1 Gyr; the step size in age is 10 Myr when the age is less than 0.1 Gyr, and is 0.1 Gyr when it ranges from 0.1 to 1 Gyr. For ease of comparison with other studies, we use a Salpeter initial mass function (IMF; Salpeter 1955). The evolution of the mass-to-light-ratio (M/L) of these models is shown in Fig. 5. As the majority of the objects in our sample have photometric information only in two bands (z_{850} and 3.6μm), we have to use an approach that is different from Yan et al. (2005). For simplicity, we only consider models of solar metallicity and zero reddening (as justified by the results of Yan et al. (2005)), and assume that all the objects are at $z = 6$.

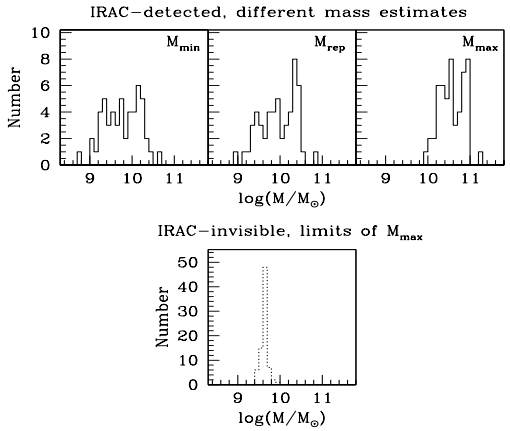

Fig. 4 The top panel displays the histograms of the stellar mass estimates of the galaxies in the IRAC-detected samples, using three different estimators as described in §4.1. The bottom panel shows the histogram of the upper limits of the stellar masses of the galaxies in the IRAC-invisible sample.

We first find the lower bound to the stellar mass (hereafter $M_{\rm min}$) of each object. If the SFH of an object is known, its ($z_{850} - m_{3.6\mu m}$) color can be used as an indicator of its age (see Fig. 2). Its mass can be derived through comparison of the observed 3.6μm magnitude to the prediction of the corresponding model at the inferred age. As we do not know what SFH a given object has, we consider the full range of models and obtain one mass estimate for each model. For each galaxy, the minimum among all these estimates is taken as its $M_{\rm min}$. While there is no other information that can further help us judge what its true mass might be, we use the median of the above estimates as the "representative mass" of this galaxy (hereafter $M_{\rm rep}$).

The maximum stellar mass that a given object can have, $M_{\rm max}$, can be calculated by assuming that the object is dominated by a maximally-old component, and thus has the maximum M/L (Fig. 3). In practice, we assume that all the flux of an object detected in the 3.6μm channel comes from a maximally-old SSP at $z = \infty$, i.e., we obtain $M_{\rm max}$by comparing its 3.6μm magnitude to the prediction given by the 1.0 Gyr-old SSP model.

These three stellar mass estimates have been calculated for all objects in the IRAC-detected sample, and their distributions are shown as histograms in the upper panel of Fig. 4. The values of $M_{\rm rep}$range from 0.09–7.0$\times10^{10}M_{\odot}$ (the median is $9.5\times10^{9}M_{\odot}$), and the corresponding ages range from 50–400 Myr (the median is 290 Myr). We can also derive the *upper limits* of $M_{\rm max}$for the IRAC-invisible sample, using the upper limits of their 3.6μm flux densities. The results are shown in the bottom panel of Fig. 4. These values range from 3.0–9.4$\times10^{9}M_{\odot}$, with the median of $4.3\times10^{9}M_{\odot}$.

4. Stacking of IRAC-invisible Objects, and the Ultra-deep Data

To further test the robustness of the conclusion that the objects in the IRAC-invisible sample are less massive, we stacked their 3.6μm images to increase the S/N of the detection. The final median stack is displayed in the left panel of Fig. 5, which shows a visible, albeit weak, source at around the center (see pixels within the circle). The magnitude of this source is 27.44 mag. For comparison, the right panel of this figure shows the stack of the same number of randomly chosen image stamps, where no detectable source at the center can be seen. Taking the median z_{850} magnitude of the IRAC-invisible sample as the z_{850} magnitude of the stacked source, we derive ($M_{\rm min}$, $M_{\rm rep}$, $M_{\rm max}$) estimates as $(1.5\times10^{8}, 2.0\times10^{8}, 5.9\times10^{9})M_{\odot}$.

The more massive objects in this sample are at the verge of being detected by the super-deep data. This is evident from the ultra-deep data, where at least one IRAC-invisible object in the super-deep observations is now detected (see Fig. 6). This object has $z_{850} = 25.99$ and $m_{3.6\mu m} = 26.90$, which corresponds to ($M_{\rm min}$, $M_{\rm rep}$, $M_{\rm max}$) of $(1.5\times10^{8}, 1.7\times10^{8}, 6.5\times10^{9}M_{\odot})$.

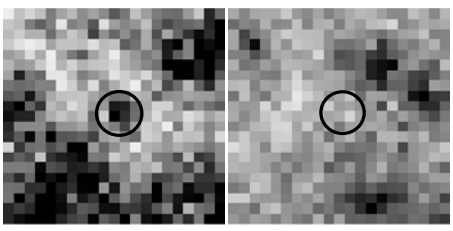

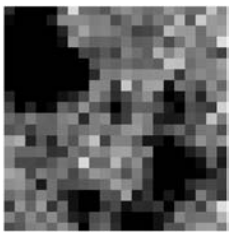

Fig. 5 (left) The 3.6μm median stack of the objects in the IRAC-invisible sample is displayed in the left panel, where there is a visible source in the middle (indicated by the circle). For comparison, the median stacks of the same number of random positions is shown in the right panel, which shows no detectable source in the middle circle.

Fig. 6 (right) At least one IRAC-invisible object in the super-deep observations has been detected by the ultra-deep data (see middle). This indicate a smooth transition of the properties of objects from one sample to the other.

5. Global Stellar Mass Density at $z \approx 6$

Our samples suffer from various sources of incompleteness. Nevertheless, we can still use our results above to obtain a lower limit of the global stellar mass density

at $z \approx 6$. This quantity, based on the ($M_{\rm min}$, $M_{\rm rep}$, $M_{\rm max}$) results given above, is (10.8,16.9,67.3)$\times 10^5 M_\odot {\rm Mpc}^{-3}$. This result is shown in Fig. 7, together with the estimates at lower redshifts (Dickinson et al. 2003). The data are shown in terms of ratios to the critical mass density, which is $1.4\times 10^{11} M_\odot {\rm Mpc}^{-3}$ in our adopted cosmology.

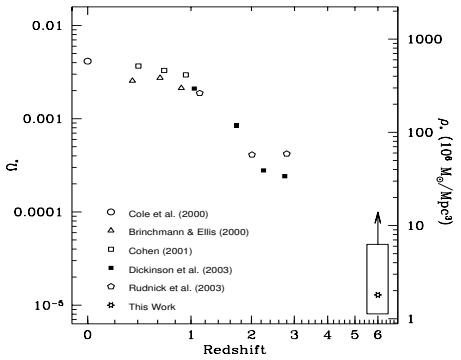

Fig. 7 The lower limit to the global stellar mass density at $z \approx 6$ based on our study is shown as the rectangle in this figure. The open star inside this rectangle shows the result based on the $M_{\rm rep}$ values, while the lower and upper boundaries are set based on the $M_{\rm min}$ and $M_{\rm max}$ values, respectively. The upward arrow indicates that these results are lower limits. The results at lower redshifts are from Cole et al. (2000), Brinchmann & Ellis (2000), Cohen (2001), Dickinson et al. (2003) and Rudnick et al. (2003). The Y-axis labels to right are in unit of $M_\odot/Mpc^3$, while the ones to the left are in terms of ratios to the critical mass density.

Acknowledgments. We thank the other members of the GOODS team who have contributed to the success of the observations and data analysis. Support for this work, part of the *Spitzer Space Telescope* Legacy Science Program, was provided by NASA through Contract Number 1224666 issued by the Jet Propulsion Laboratory, California Institute of Technology under NASA contract 1407.

References

Brinchmann, J. & Ellis, R. S. 2000, ApJ, 536, L77
Bruzual, A. G. & Charlot, S. 2003, MNRAS, 344, 1000 (BC03)
Cohen, J. G. 2001, AJ, 121, 2895
Cole, S., Lacey, C. G., Baugh, C. M., & Frenk, C. S. 2000, MNRAS, 319, 168
Dickinson, M., Paopvich, C., Ferguson, H. C., & Budavari, T. 2003, ApJ, 587, 25
Dickinson, M., et al. 2004, ApJ, 600, L99
Eyles, L. P., et al. 2005, MNRAS, 364, 443
Fazio, G. G., et al. 2004, ApJS, 154, 10
Giavalisco, M., et al. 2004a, ApJ, 600, L93
Giavalisco, M., et al. 2004b, ApJ, 600, L103
Nagamine, K., et al. 2004, ApJ, 610, 45
Rudnick, G., et al. 2003, ApJ, 599, 847
Spergel, D. N., et al. 2003, ApJS, 148, 175
Werner, M. W., et al. 2004, ApJS, 154, 1
Yan, H., et al. 2004, ApJ, 616, 63
Yan, H., et al. 2005, ApJ, 634, 109